metals

MDPI

Article

Effect of Fe Element and Ultrasonic Vibration on the Microstructure and Mechanical Properties of the Cu-TiB_2 Composites

Siruo Zhang [1,2,*], Guanglong Li [1,2], Cunhu Duan [3], Yingdong Qu [1,2], Min Cheng [4] and Shulin Dong [1,2]

[1] School of Materials Science and Engineering, Shenyang University of Technology, Shenyang 110870, China
[2] Technical Innovation Center for Lightweight and High Performance Metal Materials of Liaoning Province, Shenyang 110870, China
[3] SANY Heavy Equipment Co., Ltd., Shenyang 110020, China
[4] Key Laboratory of Solidification Control and Digital Preparation Technology (Liaoning Province), School of Materials Science and Engineering, Dalian University of Technology, Dalian 116024, China
* Correspondence: zhangsiruo@sut.edu.cn

Abstract: Cu-(Fe-Ti)-TiB_2 composites were prepared by in situ reaction and vacuum casting with and without ultrasonic vibration. The evolution of the microstructure and mechanical properties of the composite with the variation in Fe element was analyzed. The import of Fe elements could purify the matrix after in situ reaction and the formation of a nanoprecipitated phase, thus improving the strength of Cu-Fe-Ti-TiB_2 composites. Meanwhile, compared with the traditional casting process, the Cu-Fe-Ti-TiB_2 composites with ultrasonic vibration treatment exhibit uniform TiB_2 particle distribution and better properties. The tensile strength and uniform elongation of the composite with a Fe content of 0.7 wt.% reached 511 MPa and 6.02%, increasing by 14.3% and 318% compared to the unalloyed composite, respectively. The tensile strength and uniform elongation of Cu-0.7Fe-Ti-TiB_2 composite with ultrasonic vibration treatment increased to 533 MPa and 7.16%, respectively. The TiB_2 microscale particles and Fe_2Ti nanoscale precipitates with uniform distribution effectively impeded dislocation movement and recrystallization, which improved the tensile strength and stability at elevated temperatures.

Keywords: copper matrix composite; ultrasonic vibration; microalloying; microstructure; elevated temperature mechanical property

check for updates

Citation: Zhang, S.; Li, G.; Duan, C.; Qu, Y.; Cheng, M.; Dong, S. Effect of Fe Element and Ultrasonic Vibration on the Microstructure and Mechanical Properties of the Cu-TiB_2 Composites. *Metals* **2024**, *14*, 1007. https://doi.org/10.3390/met14091007

Academic Editors: Slobodan Mitrovic and Andreas Chrysanthou

Received: 5 July 2024
Revised: 15 August 2024
Accepted: 28 August 2024
Published: 2 September 2024

Copyright: © 2024 by the authors. Licensee MDPI, Basel, Switzerland. This article is an open access article distributed under the terms and conditions of the Creative Commons Attribution (CC BY) license (https://creativecommons.org/licenses/by/4.0/).

1. Introduction

Copper matrix composites (CMCs) with the desired combination of excellent mechanical properties and high-temperature stability are in significant demand in various fields such as mechanical equipment, transportation, and aerospace, including applications like resistance welding electrodes, large-scale integrated circuit lead frames, and high-speed railway contact wires [1–5]. In the past decades, particle reinforced copper matrix composites (PRCMCs) have been investigated extensively owing to their good designability, isotropy, and simple preparation processes [6–8]. Among the various types of reinforcing particles used in PRCMCs, TiB_2 particles have effectively improved their comprehensive properties because of their high hardness, high elastic modulus, high melting point, excellent wear resistance, and their good electrical and thermal conductivity; as such, they have become known as promising reinforcement particles [9–11]. Cu-TiB_2 composites have the potential to replace copper alloys, such as Cu-B alloy, in the electronics field for their high strength, better conductivity, and high-temperature resistance. The methods for preparing PRCMCs are generally divided into two major categories: the ex situ method and the in situ method. Compared with the ex situ method, in situ reaction casting exhibits better particle/matrix bonding, shorter process times, and lower costs, showing the potential for industrialization [12].

Unfortunately, the application of in situ reaction casting is still limited, which is attributed to the weak improvement in the performance of the copper matrix by single microscale particles. However, the method of further increasing the particle content to enhance performance through casting has various drawbacks. Meanwhile, incomplete reactions of Ti and B elements in the melt can also occur during the preparation of Cu-TiB_2 composites. The addition of excessive Ti improves the in situ reaction of TiB_2, but the residual Ti elements solubilize into the Cu matrix, drastically deteriorating the electrical conductivity of the composite. Alloying elements can clear up the residual trace impurities that exist in the melt after the in situ reaction process and a nanoscale precipitated phase can subsequently form during the aging process [13]. The import of hybrid-reinforced particles through alloying can significantly improve the comprehensive properties of the matrix [6,14]. However, the selection and addition of elements still require further research. Meanwhile, the reinforcing particles tend to agglomerate under the driving force of surface energy during the in situ reaction process. In recent years, applying an ultrasonic field to the melt has become an effective method. Using ultrasound during the melt generates cavitation, acoustic streaming, and other nonlinear effects, thereby mitigating the agglomeration of particles [15–17]. However, the application of ultrasound in PRCMCs is studied and analyzed less.

In this study, Fe and Ti elements were introduced into Cu-TiB_2 composites and dual-scale particles were imported through an in situ reaction and aging process, improving the mechanical properties and high-temperature stability of the composites. The introduction of ultrasonic vibration treatment significantly improved the distribution of particles in the composite, further enhancing its overall performance. The synergistic effects of Fe element and ultrasonic vibration treatment on microstructure evolution and mechanical properties were also systematically analyzed.

2. Materials and Methods

Cu-(x wt.%Fe-0.3 wt.%Ti)-1 wt.%TiB_2 composites (x = 0.35, 0.5, and 0.7, all in mass fraction hereafter) were melted through an in situ reaction method in a vacuum induction furnace equipped with an ultrasonic vibration system under an Ar atmosphere. The ultrasonic system had a maximum output power of 3 kW, a working frequency of 20 kHz, and featured a cylindrical high-temperature resistant Sialon ceramic sonotrode with a diameter of 40 mm. The melt was heated to 1250 °C and held for 10 min. Pure Fe, sponge Ti (99.99 wt.% purity), and Cu-B master alloys were sequentially added. Ultrasonic vibration treatment was introduced into the melt at 1250 °C for 3 min, and the melt was poured into a metal mold to form as-cast ingots after ultrasonic vibration treatment. Two series of specimens with and without ultrasonic vibration treatment were prepared in this study. The as-cast ingots were subjected to homogenization at 960 °C for 24 h and were then hot-rolled at 850 °C with a total deformation of 30%. After hot-rolling, the Cu-Fe-Ti-TiB_2 ingots underwent a solution treatment at 1000 °C for 4 h. Prior to rolling at room temperature, it was necessary to remove the oxide layer from the surface of the ingot, and the total rolling reduction of all the samples was 90%. The ingots were subjected to isothermal aging treatments at 450 °C and 500 °C.

The electrical conductivity test was conducted using a Sigmascope SMP 350 eddy current conductivity tester (Sigmascope SMP 350, Sindelfingen, Germany). Each sample was tested 10 times and average values were reported. Hardness testing was performed using the Vickers hardness tester (MH-50, Beijing, China) with a loading force of 100 gf and a pressure holding time of 15 s. The hardness test was conducted at least seven time per sample and the average result was obtained by excluding the maximum and minimum values. X-ray diffraction (XRD) analysis was carried out between 20° and 100° at room temperature using an EMPYREAN diffractometer equipped with a Cu/Kα radiation (EMPYREAN, British). Prior to the characterization of the microstructure, the surface of each specimen was polished with 240–2000 grit sandpaper and then electrolytically polished in a solution with 2% HCL, 3% $FeCl_3$, and 95% C_2H_5OH for 30 s. The microstructure

was characterized using an optical microscope (OM, Olmpus GX51, Tokyo, Japan) and a scanning electron microscope (SEM, JSM-7900F, Tokyo, Japan). Microstructure and micro-area composition analysis of samples were performed using electron probe microanalysis (EPMA, JXA8530F PLUS, JEOL, Tokyo, Japan). A transmission electron microscope (TEM, Talos F200x, Dreieich, Germany) was used for detailed microstructure analysis, operating at 200 kV. The specimens for TEM were thinned by grind and ion-beam thinning (Gatan 695, Pleasanton, CA, USA). Room temperature tensile tests were performed using an UTM-5105 tensile testing machine equipped with video extensometer (NCM-2D, Shanghai, China). High-temperature tensile tests at 100 °C and 300 °C were carried out using an UMS-100 (SUNS, Shenzhen, China) tensile testing machine, with a preheating time of 10 min in the environmental chamber. The strain rate of room and elevated temperature tensile tests maintained 10^{-3} s^{-1}.

3. Results

The XRD phase analysis of the cast composite is shown in Figure 1. From Figure 1a, it is observed that only two phases (Cu and TiB_2) are detected in the composite prepared via in situ reaction. Additionally, based on the XRD spectra of the composite within the range 73.6°–74.6°, as shown in Figure 1b, it is evident that the Cu peak in the composite with addition of Ti and Fe elements shifts towards the left compared to the composite without these elements. Moreover, the extent of the Cu peak shift increases in the composite with the increase in Fe content, which indicates that Ti and Fe atoms dissolve into the Cu matrix. No other phases containing both Fe and Ti elements were detected.

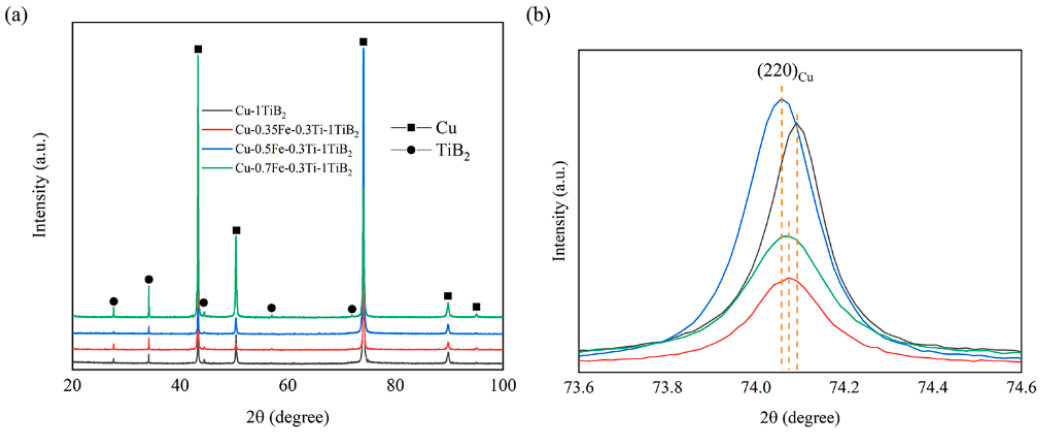


Figure 1. XRD patterns of as-cast Cu-1TiB_2 and Cu-*x*Fe-0.3Ti-1TiB_2 composites: (**a**) 20°–90°; (**b**) 73.6°–74.6°.

Surface scanning analysis was conducted on the cast Cu-Fe-Ti-TiB_2 composite and the results are depicted in Figure 2. Four elements (Cu, Ti, B, and Fe) are consistently detected within the three different Fe content variations in the composites. Moreover, the presence of an Fe-rich phase within the Cu matrix is visible in the images, which contributes to the decreasing solubility of Fe in Cu as the temperature drops. Fe elements beyond the solubility limit at room temperature exist within the matrix in the form of an Fe-rich phase. The volume fraction of the Fe-rich phase within the matrix also increases with the increase in Fe content, as shown in Figure 2a–c. These Fe-rich phases are mostly found in association with TiB_2 particles.

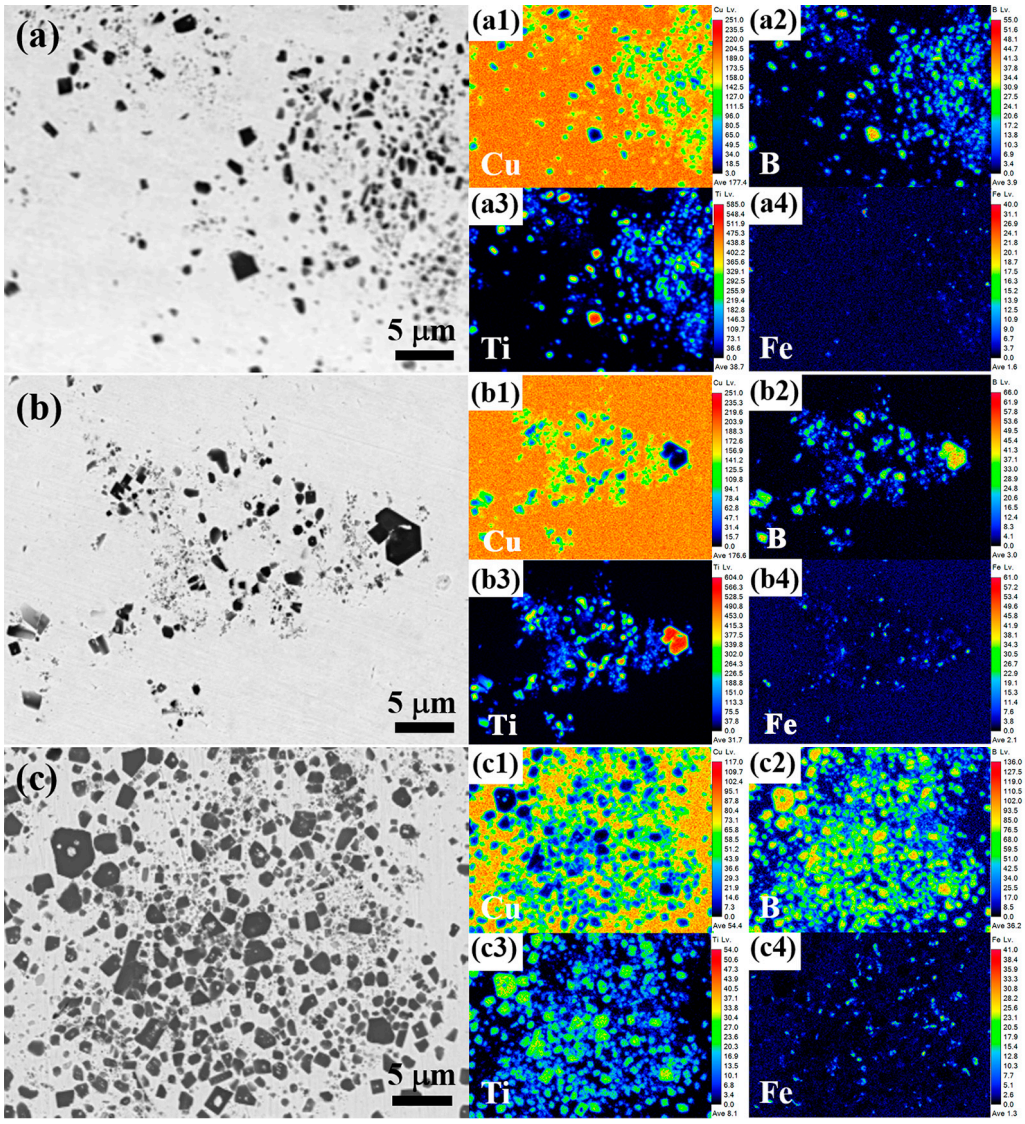


Figure 2. EPMA mapping analysis of element distribution in as-cast Cu-1TiB_2 and Cu-*x*Fe-0.3Ti-1TiB_2 composites: (**a**) x = 0.35, (**a1**–**a4**) distribution of Cu, B, Ti and Fe element; (**b**) x = 0.5, (**b1**–**b4**) distribution of Cu, B, Ti and Fe element; (**c**) x = 0.7, (**c1**–**c4**) distribution of Cu, B, Ti and Fe element. (**a1**–**a4**,**b1**–**b4**,**c1**–**c4**).

Figure 3 illustrates the variation in electrical conductivity and hardness for different Fe contents under varying aging conditions. The electrical conductivity of the composites increases with prolonged aging time at both 450 °C and 500 °C aging temperatures. A rapid increase in conductivity occurs initially, followed by a gradual slowdown as the aging time increases. As the Fe content increases, the electrical conductivity of the composite decreases, while hardness demonstrates an inverse trend. The composite with an Fe content of 0.35 wt.% reaches a peak hardness of 143.3 HV after aging for 2 h, whereas composites with Fe contents of 0.5 wt.% and 0.7 wt.% display continuously increasing hardness with longer aging durations, as shown in the hardness evolution during isothermal aging at 450 °C (Figure 3b). Regarding the hardness variation during isothermal aging at 500 °C (Figure 3d), the composite with an Fe content of 0.35 wt.% exhibits an overall decreasing trend in hardness, indicating an obvious over-aging. On the contrary, the hardness of composites with Fe contents of 0.5 wt.% and 0.7 wt.% initially rises and then declines after prolonged aging time. The composites with Fe contents of 0.5 wt.% and 0.7 wt.% reach peak hardness values of 151.2 HV and 156.3 HV after 1 h of aging at 500 °C, respectively. Therefore, the optimal aging conditions are selected as 450 °C for 2 h for the composite

with an Fe content of 0.35 wt.% and 500 °C for 1 h for the composites with Fe content of 0.5 wt.% and 0.7 wt.%.

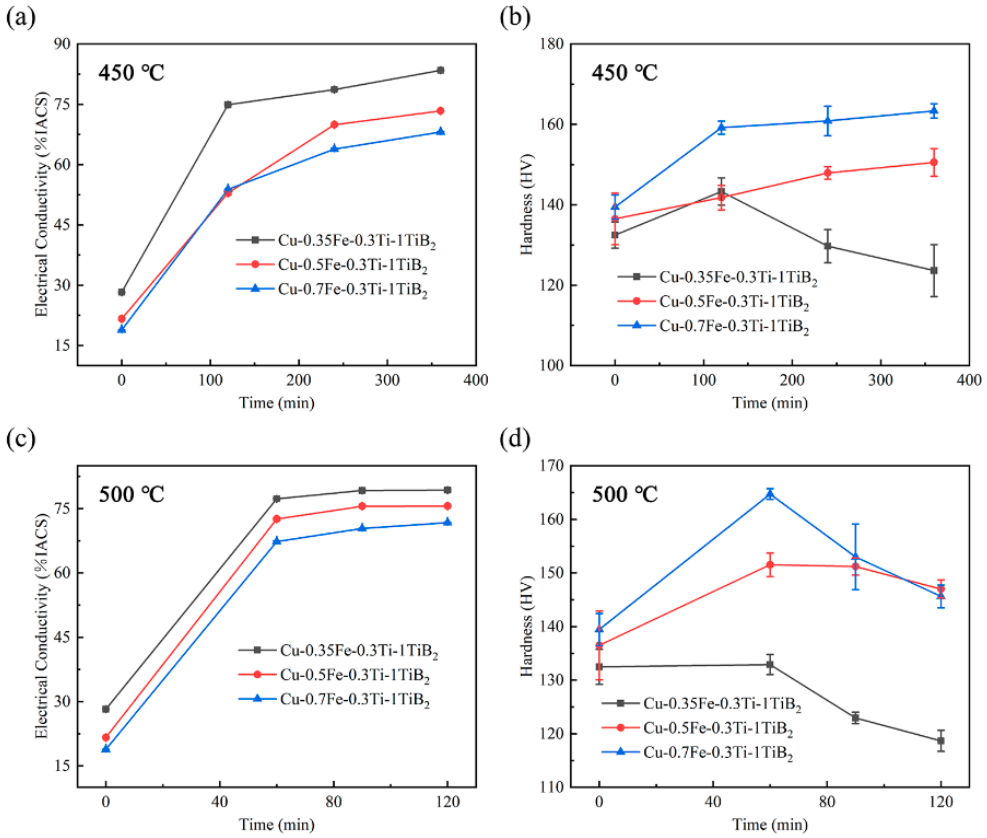


Figure 3. Curves of electrical conductivity and hardness of Cu-Fe-Ti-TiB_2 composites with aging time at different aging temperatures: (**a**) Electrical conductivity at 450 °C; (**b**) Hardness at 450 °C; (**c**) Electrical conductivity at 500 °C; (**d**) Hardness at 500 °C.

The surface scanning analysis of the as-aged Cu-Fe-Ti-TiB_2 composite is presented in Figure 4. The Fe-rich phase, which initially appeared within the matrix of the as-cast composite, has essentially disappeared, having precipitated from the Cu matrix in the form of nanoscale FeTi-rich phases after solid solution and aging treatment. The tensile strength of the as-aged Cu-Fe-Ti-TiB_2 composites compared with the unalloyed as-rolled Cu-TiB_2 composite is depicted in Figure 5. The elongation of composites increases with the increase of Fe content, surpassing the unalloyed composite significantly. The composite with an Fe content of 0.35 wt.% exhibits lower strength compared to the unalloyed composite, whereas the strength of the composites with Fe content of 0.5 wt.% and 0.7 wt.% surpass that of the Cu-TiB_2 composites. The tensile strength of the composites with Fe content of 0.5 wt.% and 0.7 wt.% reaches 501 MPa and 511 MPa, respectively, increasing by 12.1% and 14.3% compared to the unalloyed composite.

Figure 6 presents the XRD diffraction analysis of the as-cast Cu-0.7Fe-0.3Ti-1TiB_2 composite with and without UVT. The analysis reveals that only two phases (Cu and TiB_2) occur within the composite, which corresponds to the as-cast composite. The result suggests that UVT has less influence on the formation of phases in the casting process. Figure 7 displays SEM images of as-cast Cu-0.7Fe-0.3Ti-1TiB_2 composites with and without UVT. The distribution of TiB_2 particles in the composite with UVT shows a significant improvement, exhibiting a uniform dispersion throughout the entire Cu matrix, as shown in Figure 7a,c. In the magnified images (Figure 7b,d), TiB_2 particles are seen to be clustered in the composite without UVT, while the treated composite shows a more dispersed particle distribution. Figure S1 depicts mapping analysis of the as-cast Cu-0.7Fe-0.3Ti-1TiB_2 composite with UVT.

It is evident that the Ti element primarily combines with the B element in the form of TiB_2 particles, and that Fe elements are predominantly found around the TiB_2 particles.

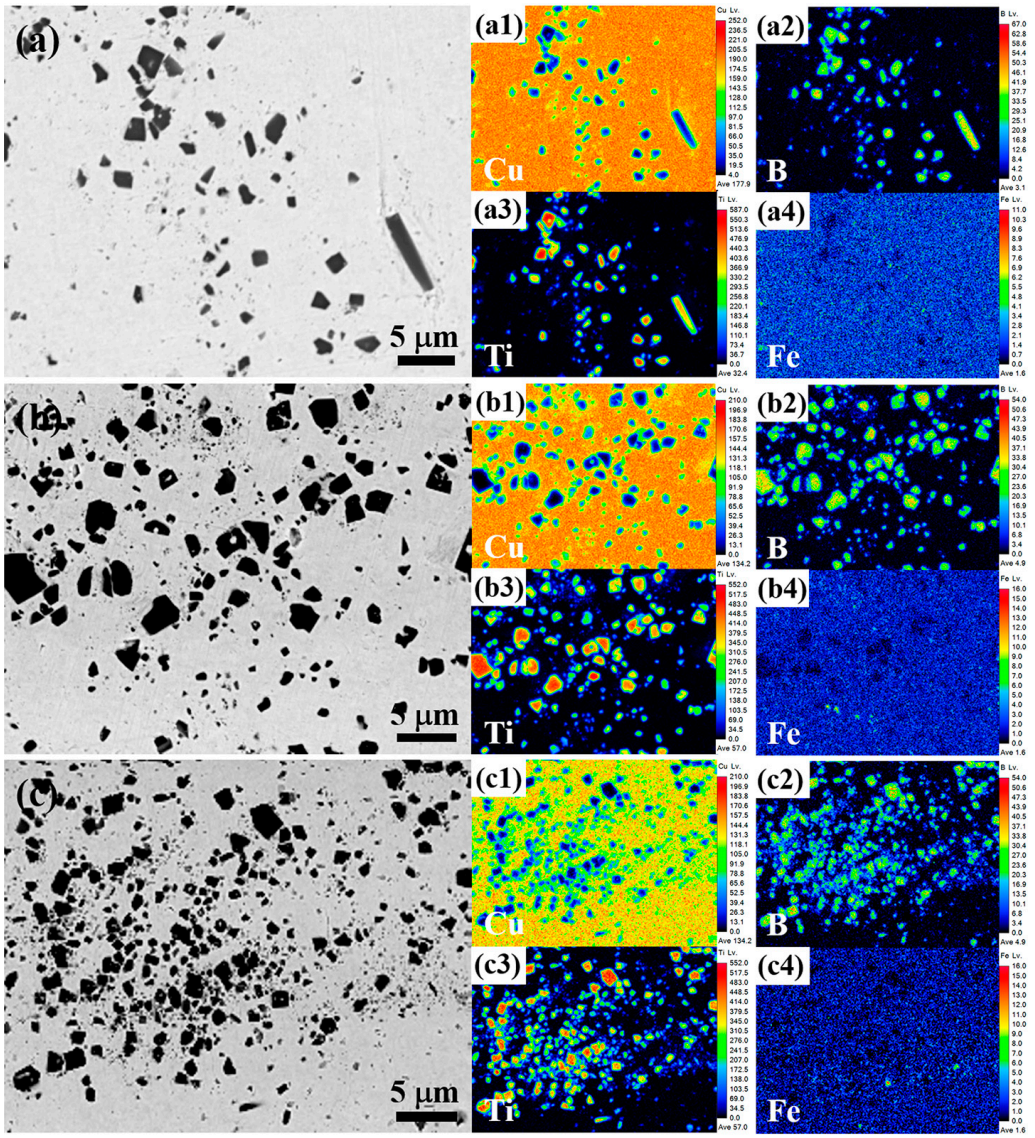


Figure 4. EPMA mapping analysis of element distribution in as-aged Cu-*x*Fe-0.3Ti-1TiB_2 composites: (**a**) x = 0.35, (**a1**–**a4**) distribution of Cu, B, Ti and Fe element; (**b**) x = 0.5, (**b1**–**b4**) distribution of Cu, B, Ti and Fe element; (**c**) x = 0.7, (**c1**–**c4**) distribution of Cu, B, Ti and Fe element. (**a1**–**a4**,**b1**–**b4**,**c1**–**c4**).

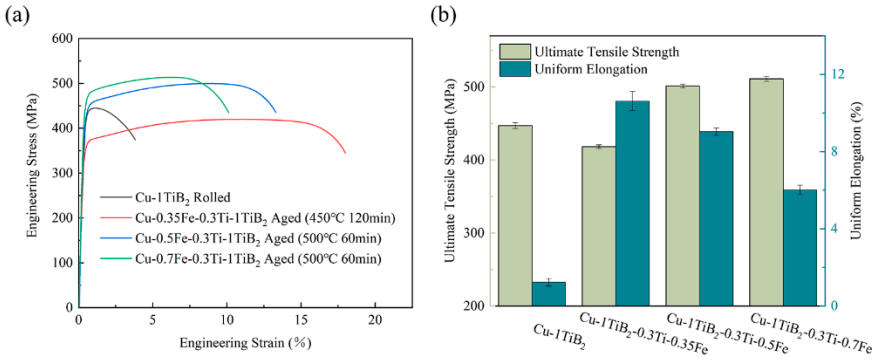


Figure 5. (**a**) Tensile curves and (**b**) mechanical properties of Cu-1TiB_2 and Cu-*x*Fe-0.3Ti-1TiB_2 composites under different states.

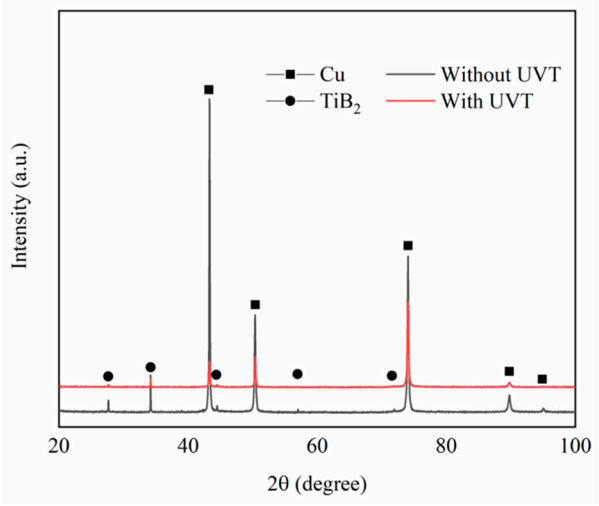


Figure 6. XRD patterns of as-cast Cu-0.7Fe-0.3Ti-1TiB_2 composites with and without UVT.

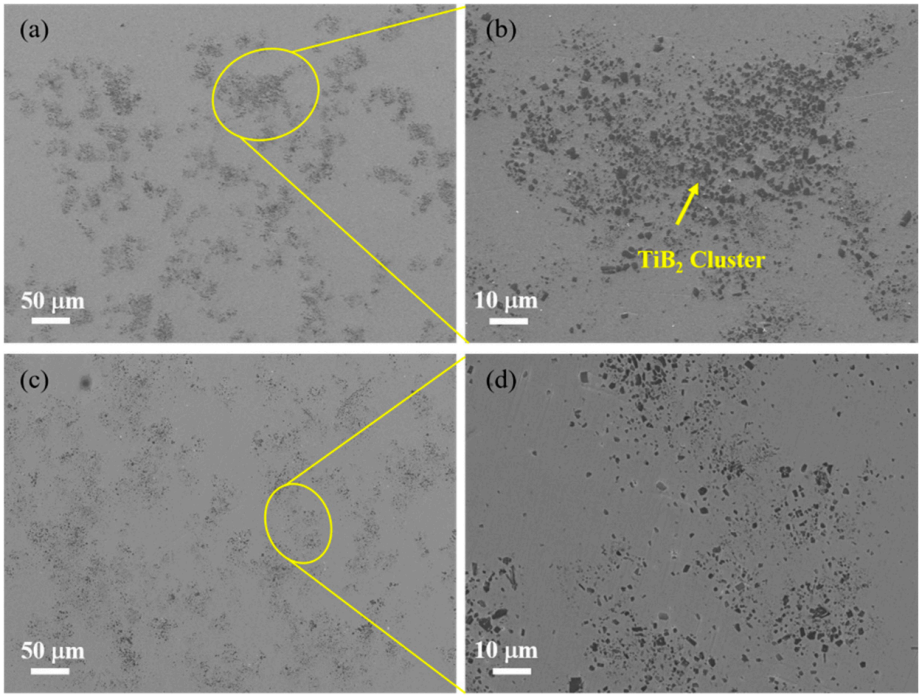


Figure 7. SEM micrographs of as-cast Cu-0.7Fe-0.3Ti-1TiB_2 composites: (**a**,**b**) without UVT; (**c**,**d**) with UVT.

The Cu-0.7Fe-0.3Ti-1TiB_2 composite with UVT was subjected to deformation and heat treatment, followed by aging under different conditions. Figure 8 illustrates the variations in electrical conductivity and hardness during aging at 450 °C and 500 °C. The composite exhibits a low electrical conductivity of only 18.8% IACS after solid solution and cold rolling processing. The hardness of the composite exhibits a consistent increase with prolonged aging time at 450 °C. The trend of hardness rises initially and then declines subsequently during isothermal aging at 500 °C, reaching a peak value of 167.8 HV after 1 h of aging. The hardness of the composite achieves peak value more rapidly than at 450 °C, indicating that the elevated aging temperature improves the precipitation process of Fe and Ti from the Cu matrix. Hence, the optimal aging condition is selected as 500 °C, 1 h for the Cu-0.7Fe-0.3Ti-1TiB_2 composite.

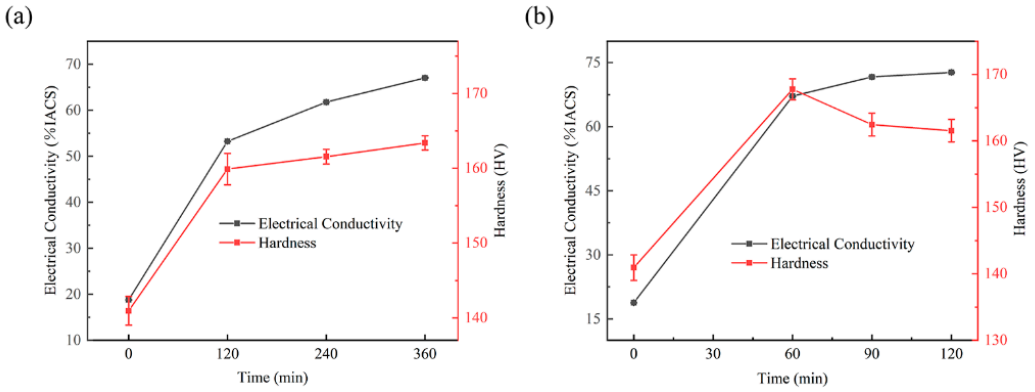


Figure 8. Curves of electrical conductivity and hardness of the Cu-0.7Fe-0.3Ti-1TiB_2 composite with UVT aging at different aging temperatures: (**a**) 450 °C; (**b**) 500 °C.

Figure 9 displays OM images of the as-aged Cu-0.7Fe-0.3Ti-1TiB_2 composite with and without UVT. The TiB_2 particles within the composite are parallel to the rolling direction after the rolling deformation process, and clusters of TiB_2 particles are elongated along the rolling direction in the as-cast composite, as shown in Figure 9a. It is evident that the particle distribution in composites with UVT is more uniform, indicating that cavitation and acoustic streaming effects contribute to the dispersion of particle clusters and retain a better dispersion of TiB_2 particles even after subsequent deformation and heat treatment, as shown in Figure 9b. Figure S2 shows the microstructure and elemental surface scan of the as-aged Cu-0.7Fe-0.3Ti-1TiB_2 composite with UVT. The Fe-rich phase within the as-aged composite has essentially disappeared and the Fe and Ti elements precipitate from the matrix to form nanoscale precipitates after solid solution and aging treatments.

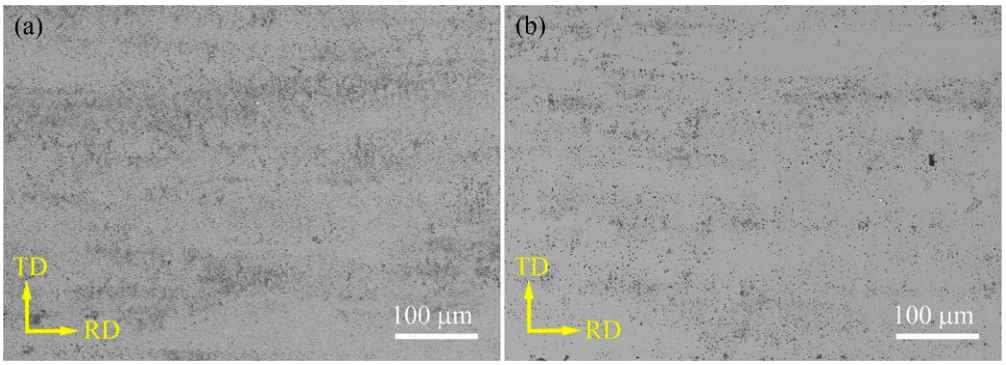


Figure 9. OM micrographs of as-aged Cu-0.7Fe-0.3Ti-1TiB_2 composites: (**a**) without UVT; (**b**) with UVT.

TEM analysis was conducted on the as-aged Cu-0.7Fe-0.3Ti-1TiB_2 composite with UVT and the results are depicted in Figure 10. From Figure 10a, a large number of elongated deformation bands along the rolling direction and dislocation tangle can be observed within the composite after rolling process. Additionally, cellular structures are also present within the composite, as shown in Figure 10b. Figure 10c,d clearly illustrate abundant nanoscale precipitates within the Cu matrix, indicating a clearer depiction of the interaction between the nanoscale precipitates and dislocations. Figure 10e presents a high-resolution image of the nanoscale precipitates, which were subjected to a rapid Fourier transformation and calibrated with previous literature, confirming the nanoscale precipitates as Fe_2Ti phases.

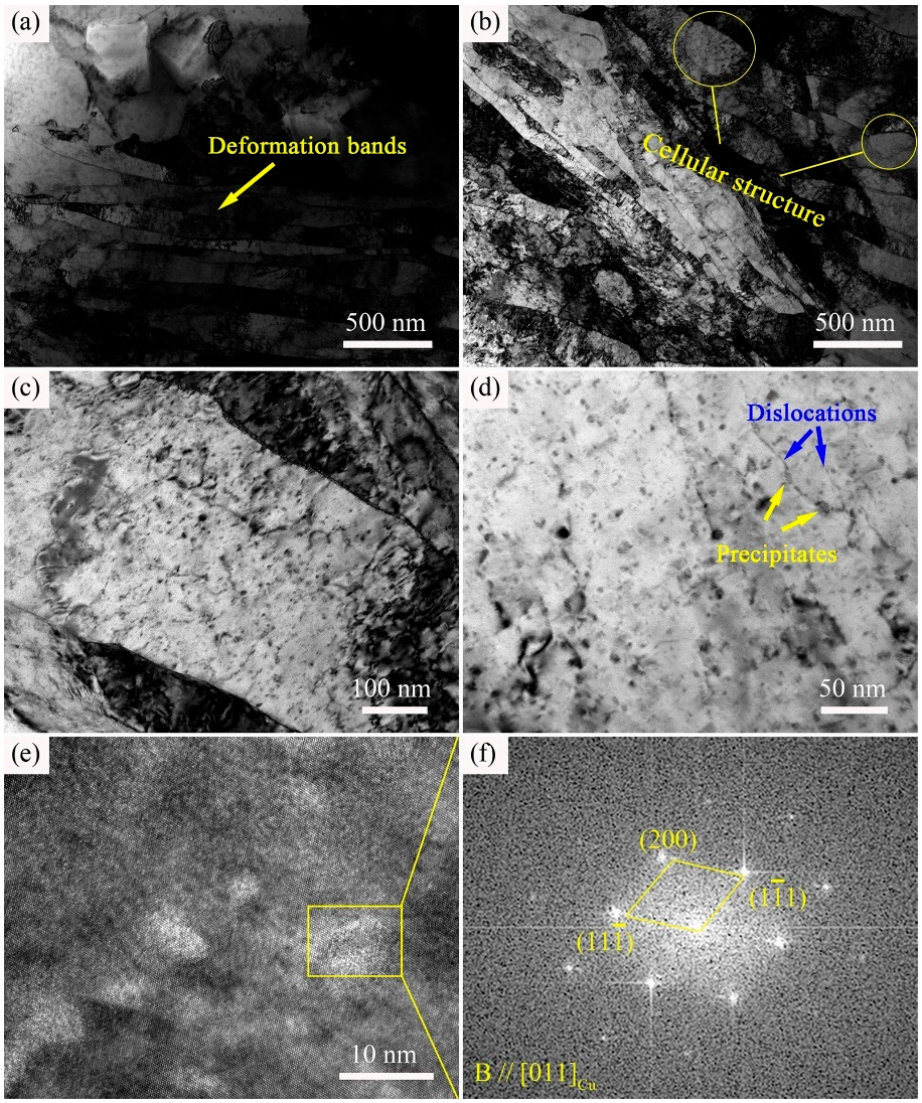


Figure 10. TEM images of as-aged Cu-0.7Fe-0.3Ti-1TiB_2 composite with UVT: (**a**) deformation bands; (**b**) cellular structure; (**c**) nanoprecipitates; (**d**) nanoprecipitates and dislocations; (**e**) HRTEM image of nanoprecipitate; (**f**) fast Fourier transform of nanoprecipitate in (**e**).

Tensile experiments were performed on the as-aged Cu-0.7Fe-0.3Ti-1TiB_2 composite with and without UVT, as shown in Figure 11. The strength and elongation of the composite with UVT are improved simultaneously, as shown in Figure 11a. According to Figure 11b, the composite without UVT exhibits a tensile strength and uniform elongation of 511 MPa and 6.0%, respectively, whereas the composite with UVT shows an increase in tensile strength and uniform elongation, reaching 533 MPa and 7.2%, representing improvements of 4.3% and 18.9%, respectively.

Figure 12 illustrates the tensile curves of the composites with and without UVT at 100 °C and 300 °C. The composites with and without UVT maintain relatively high strength at 100 °C, with reductions of 6.7% and 8.5%, respectively, which is significantly higher than tensile strength of the Cu-TiB_2 composite. However, the average tensile strengths of composites with and without UVT at 300 °C are 332 MPa and 321 MPa, respectively, showing significant improvement compared to the unalloyed composite.

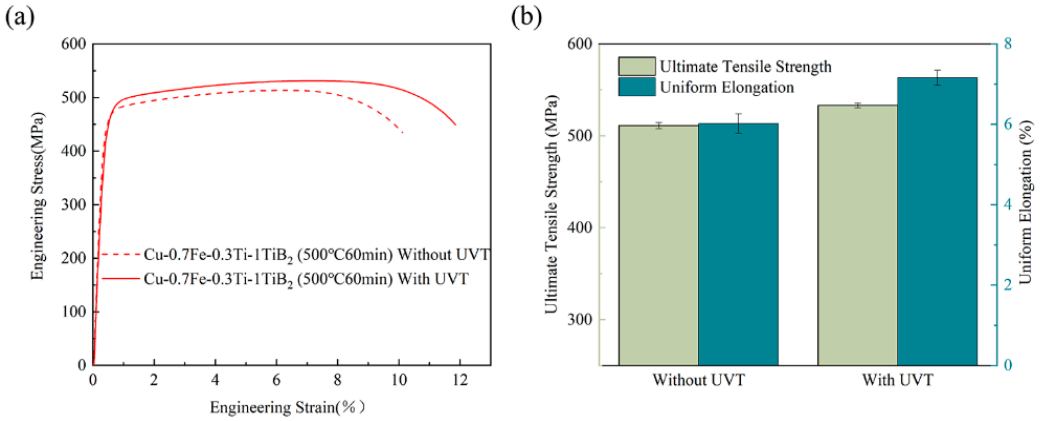


Figure 11. (**a**) Tensile curves and (**b**) mechanical properties of as-aged Cu-0.7Fe-0.3Ti-1TiB_2 composites.

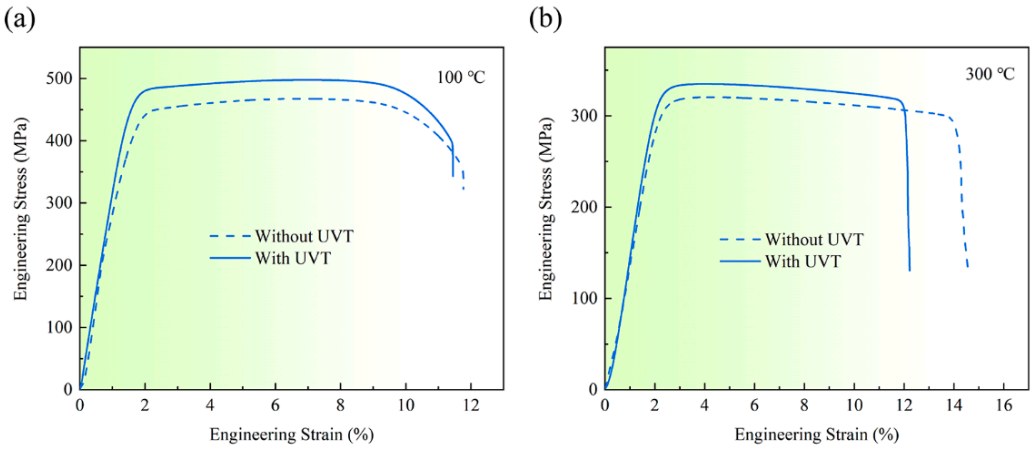


Figure 12. Tensile curves of as-aged Cu-0.7Fe-0.3Ti-1TiB_2 composites at different temperatures: (**a**) 100 °C; (**b**) 300 °C.

4. Discussion

4.1. Effects of Fe on Microstructural Evolution and Mechanical Properties

Introducing Fe and excess Ti elements into Cu-TiB_2 composites facilitates the generation of in situ particles within the in situ process, enhancing the utilization efficiency of B elements. Meanwhile, the addition of Fe and Ti elements can precipitate in terms of thermodynamics, leading to an increase tensile strength and electrical conductivity in the aging process. During the casting and solidification processes, the introduction of Fe and Ti elements leads to a significant solid solution within the composite. As the temperature decreases, the solubility of Fe in Cu drastically diminishes, causing the excess Fe to convert into the form of Fe-rich phases [18]. With an increase in Fe content, the volume fraction of Fe-rich phases exhibits a corresponding rise, coexisting with TiB_2 particles in the form of point-like shape. The coexistence of Fe-rich phases and TiB_2 particles is primarily due to the higher concentration of Ti near the TiB_2 particles, where excess Ti tends to react with Fe, forming Fe-Ti compounds [13]. Moreover, the similar thermal expansion coefficients and good wetting properties between Fe and TiB_2 particles contribute to the enrichment of Fe near the TiB_2 particles. The Fe elements in solid solution and the Fe-rich phases undergo significant phase transformations during subsequent deformation and heat treatment processes.

After subsequent solution treatment, deformation, and aging processes, the Fe-rich phases in the as-cast composite significantly diminish and the size reduces to submicron levels. EPMA analysis confirms the presence of nanoscale Fe-Ti-rich precipitates within the composite matrix. In this study, the optimal aging condition for the Cu-Fe-Ti-TiB_2 composite material was determined to be 500 °C for 1 h. Numerous spherical precipitates

occur within the composite after aging treatment, ranging in size from 5 to 10 nanometers. A steak-like feature in the as-aged composites is identified through high-resolution observation, and the precipitates are confirmed to be Fe_2Ti phases [19]. Meanwhile, abundant deformation bands and dislocation structures are also observed within the composite. Extensive precipitates distribute close to these deformation bands, which act as nucleation sites for precipitates during the aging process, leading to promotion of precipitation [20,21]. Furthermore, the presence of substantial precipitates effectively impedes dislocation slip, and the interaction between precipitates and dislocations affects the microstructure of the composites, enhancing the mechanical properties of composites significantly.

As a result of the variation in added Fe element, the properties of the composite change significantly during the aging process. During aging, supersaturated Fe and Ti solute atoms precipitate within the Cu matrix and the temperature of aging treatment coincides with the temperature range for recrystallization of the composite, thus leading to the coexistence of precipitation strengthening and recrystallization softening. In composites with lower Fe content, the volume fraction of precipitates is limited, resulting in weaker strengthening effects. Meanwhile, a lower quantity of precipitates results in weaker hindrance against recrystallization, leading to higher degrees of recrystallization and strength reduction in the composite. In composites with an Fe content of 0.5 wt.% and 0.7 wt.%, the volume fraction of precipitates increases significantly after aging treatment, obstructing the motion of dislocations [22]. Dislocation lines bend around these nano-sized precipitates, forming dislocation loops under sustained external stress [23]. Therefore, the hinderance effect of nano-sized precipitates on dislocations significantly strengthens the composite [18]. Moreover, the presence of increased precipitates also impedes recrystallization in the aging treatment, leading to further enhancement of strength. With increasing aging temperature and prolonged aging time, the strength of the composite exhibits a trend of initial increase followed by a decrease, which indicates that the presence of nanoscale precipitates enhances the resistance of deformation in the initial stage and that the coarsening of these precipitates weakens the strengthening effect on the matrix with prolonged aging. The deformation structure of the composite undergoes softening at high temperatures and over a long aging time, which leads to a decrease in hardness, indicating the existence of an optimum aging process for the composite [20].

For high-temperature mechanical properties of composites, the addition of Fe elements enhances the strength performance significantly at elevated temperatures, considerably broadening the application range of the composites. The aging process introduces nanoscale precipitates into the alloyed composite, which effectively pin dislocations at 100 °C, hindering the recovery and resulting in a notable reduction in strength degradation. During tensile testing at 300 °C, the composite is subjected to dynamic recrystallization, while the nanoscale precipitates suppress recrystallization nucleation, enhancing the resistance of softening at high temperature.

The electrical conductivity of the composites also exhibits systematic changes during isothermal aging. With increasing aging temperature and prolonged aging time, the electrical conductivity of the composites shows an upward trend. According to the Matthiessen's rule, electron scattering caused by solute atoms significantly affects resistivity [24]. By inducing the precipitation during the aging process, electron scattering caused by solute atoms can be alleviated and the precipitation of solute atoms improves the electrical conductivity of the composite [25]. The volume fraction of nanoscale precipitates increases in the aging process, leading to a decrease in solute atom concentration and a continuous rise in the electrical conductivity of the composite [26]. Simultaneously, the composite undergoes recovery and recrystallization during aging treatment, reducing dislocation density, which also contributes to an increase in electrical conductivity.

4.2. Effects of Ultrasonic Vibration on Microstructural Evolution and Mechanical Properties

In the in situ reaction process of copper matrix composites, the small reinforcing particles suffer from surface forces, such as van der Waals forces, and capillary forces, which

surpass inertial forces due to their large surface area, leading to particle agglomeration within the matrix [27]. Meanwhile, the agglomerated reinforcing particles further contribute to the uneven distribution of Fe-rich phases, resulting in noticeable particle aggregation in the as-aged composites after subsequent deformation and heat treatment processes. The ultrasonic vibration is applied to the in situ reaction of the Cu-0.7Fe-0.3Ti-1TiB_2 composite, generating significant cavitation effects within the Cu melt. The cavitation effects introduce the nucleation, growth, and collapse of cavities within the Cu melt, generating instantaneous high temperature, high pressure, and high-speed melt microjets [15,16,28,29]. These instantaneous effects lead to the deagglomeration of TiB_2 particle clusters caused by the generation of capillary effects. Another nonlinear effect generated by acoustic streaming facilitates the movement of TiB_2 particles within the entire melt through ultrasonic waves, dispersing TiB_2 particles and preventing the formation of particle clusters [17]. Hence, the agglomeration of TiB_2 particles improves significantly under the combined effects of cavitation and acoustic streaming, resulting in a more dispersed and uniform distribution within the Cu matrix [30,31]. Furthermore, the improvement of aggregation also leads to a more uniform distribution of Fe-rich phases, significantly reducing stress concentration in the composite. The extensive particle agglomeration is elongated along the rolling direction after heat treatment and deformation and the composite with UVT exhibits a more uniform trend, significantly reducing the degree of particle agglomeration. Uniformly distributed reinforcement particles can hinder grain boundary and dislocation slip during deformation, resulting in refining grains and proliferating dislocations [32]. Moreover, reinforced particles with better distribution can also promote the formation of precipitates during aging. All these discussions indicate that copper matrix composites inherit distinct characteristics from UVT, optimizing the microstructure of as-aged composites and enhancing their properties significantly.

Reinforced particle agglomeration within the composite cannot effectively act as Orowan strengthening phases due to their increased size. The effectiveness of Orowan strengthening is also related to the volume fraction of the reinforcing particles [33]. Therefore, the presence of agglomerates hinders the improvement of strength and stress concentration and is more likely to occur near these agglomerates, leading to the initiation of early microcracks, thereby deteriorating the strength and elongation of the composite significantly. After UVT, the situation of agglomeration improves under the combined effects of cavitation and acoustic streaming, promoting a more uniform distribution of particles, increasing the effective volume fraction of TiB_2 reinforcing phases, and consequently enhancing the strength compared to the composite without UVT [34]. Simultaneously, the deagglomeration process reduces stress concentration effectively, suppressing the initiation of early microcracks during deformation and increasing the elongation of composite [35]. In the alloyed composite with UVT, Fe elements concentrate near uniform distribution of TiB_2 particles during subsequent deformation and aging processes.

The strength of the composite with UVT also exhibits better strength at elevated temperatures, which is primarily due to the simultaneous occurrence of work hardening and recovery within the composite at 100 °C. Moreover, TiB_2 microscale particles and Fe_2Ti nanoscale precipitates with uniform distribution exhibit a pronounced ability to impede dislocation movement, resulting in a smaller decline in the strength of the composite. However, significant dynamic recovery and recrystallization occur within the composite at 300 °C. At this stage, dynamic recrystallization becomes the primary softening mechanism and a notable reduction in dislocation density occurs, leading to a substantial decrease in strength and a significant increase in plasticity compared to performance at room temperature [20]. Thus, the strength of the composite with UVT remains higher than that of the composite without UVT due to the hindrance caused by TiB_2 particles and nano-precipitates against dynamic recrystallization [18].

5. Conclusions

A high-performance sample of the Cu-TiB_2 composite was prepared through the addition of Fe elements and the novel method of ultrasonic vibration treatment. The evolution of microstructure and mechanical properties of the composite with the variation of Fe element and ultrasonic vibration was examined using advanced characterization methods. The main conclusions are as follows:

(1) The combination of Fe and Ti alloying with aging treatment contributes to the enhancement of strength and elongation in Cu-TiB_2 composites. The tensile strength and uniform elongation of the composite with an Fe content of 0.7 reach 511 MPa and 6.02%, respectively, achieving a comprehensive property compared with the unalloyed composite.

(2) Ultrasonic vibration treatment can improve the strength and plasticity of composites simultaneously. The as-aged Cu-0.7Fe-0.3Ti-1TiB_2 composite with ultrasonic vibration treatment exhibits a tensile strength and uniform elongation of 533 MPa and 7.2%, respectively, representing an increase of 4.3% and 18.9% compared to the composite without ultrasonic vibration treatment.

(3) The combined effects of cavitation and acoustic flow improve the distribution of particles in the as-cast composite through ultrasonic vibration, and the TiB_2 microscale particles and Fe_2Ti nanoscale precipitates with uniform distribution effectively impede dislocation movement and delay recrystallization, which improves the tensile strength and stability at elevated temperature.

Supplementary Materials: The following supporting information can be downloaded at: https://www.mdpi.com/article/10.3390/met14091007/s1, Figure S1: EPMA mapping analysis of element distribution in as-cast Cu-0.7Fe-0.3Ti-1TiB_2 composite with UVT; Figure S2: EPMA mapping analysis of element distribution in as-aged Cu-0.7Fe-0.3Ti-1TiB_2 composite with UVT.

Author Contributions: Conceptualization, S.Z., G.L. and C.D.; methodology, S.Z. and G.L.; software, S.Z., M.C. and C.D.; validation, S.Z., C.D. and G.L.; formal analysis, S.Z. and G.L.; investigation, S.Z., M.C., C.D. and Y.Q.; data curation, S.Z., S.D. and G.L.; writing—original draft preparation, S.Z.; writing—review and editing, S.Z. and G.L.; supervision, Y.Q.; project administration, Y.Q.; funding acquisition, S.Z. and G.L. All authors have read and agreed to the published version of the manuscript.

Funding: This study was financially supported by the National Natural Science Foundation of China (Nos. 52301061 and 52204394), Joint Fund Project of Science and Technology Plan of Liaoning Province (No. 2023-MSLH-250), Science and Technology Program of Liaoning Provincial Department of Education (No. JYTQN2023286).

Data Availability Statement: The original contributions presented in the study are included in the article/Supplementary Materials, further inquiries can be directed to the corresponding author.

Conflicts of Interest: Author Cunhu Duan was employed by the company SANY Heavy Equipment Co., Ltd. The remaining authors declare that the research was conducted in the absence of any commercial or financial relationships that could be construed as a potential conflict of interest.

References

1. Feng, J.; Song, K.; Liang, S.; Guo, X.; Li, S. Mechanical properties and electrical conductivity of oriented-SiC-whisker-reinforced Al_2O_3/Cu composites. *J. Mater. Res. Technol.* **2022**, *20*, 1470–1480. [CrossRef]
2. Xiao, Z.; Huang, Y.; Chen, C.; Li, Z.; Gong, S.; Huang, Y.; Zhang, C.; Zhang, X. Effects of thermal treatments on the residual stress and micro-yield strength of Al_2O_3 dispersion strengthened copper alloy. *J. Alloys Compd.* **2019**, *781*, 490–495. [CrossRef]
3. Liang, S.; Li, W.; Jiang, Y.; Cao, F.; Dong, G.; Xiao, P. Microstructures and properties of hybrid copper matrix composites reinforced by TiB whiskers and TiB_2 particles. *J. Alloys Compd.* **2019**, *797*, 589–594. [CrossRef]
4. Fan, X.; Huang, X.; Liu, Q.; Ding, H.; Wang, H.; Hao, C. The microstructures and properties of in-situ ZrB_2 reinforced Cu matrix composites. *Results Phys.* **2019**, *14*, 102494. [CrossRef]
5. Wang, X.; Jie, J.; Liu, S.; Dong, Z.; Yin, G.; Li, T. Growth mechanism of primary Ti_5Si_3 phases in special brasses and their effect on wear resistance. *J. Mater. Sci. Technol.* **2021**, *61*, 138–146. [CrossRef]

6. Chen, W.; Gao, G.; Meng, X.; Zhao, X.; Jiang, Y.; Wang, M.; Li, Z.; Xiao, L. Microstructure, properties and strengthening mechanism of Cu-TiB_2-Al_2O_3 composite prepared by liquid phase in-situ reaction casting. *J. Alloys Compd.* **2022**, *912*, 165170. [CrossRef]
7. Zhao, H.; Feng, Y.; Zhou, Z.; Qian, G.; Zhang, J.; Huang, X.; Zhang, X. Effect of electrical current density, apparent contact pressure, and sliding velocity on the electrical sliding wear behavior of Cu–Ti_3AlC_2 composites. *Wear* **2020**, *444–445*, 203156. [CrossRef]
8. Bashir, K.; Gupta, D.; Jain, V. Microstructural investigation of variable tungsten reinforcement in copper-based composite microwave castings. *Int. J. Metalcast.* **2024**. [CrossRef]
9. Feng, J.; Song, K.; Liang, S.; Guo, X.; Jiang, Y. Electrical wear of TiB_2 particle-reinforced Cu and Cu–Cr composites prepared by vacuum arc melting. *Vacuum* **2020**, *175*, 109295. [CrossRef]
10. Cao, F.; Dong, G.; Jiang, Y.; Xiao, P.; Wang, T.; Liang, S. Effect of La addition on microstructures and properties of TiB_2(-TiB)/Cu hybrid composites prepared by in situ reaction. *Mater. Sci. Eng. A* **2020**, *789*, 139605. [CrossRef]
11. Kim, J.H.; Yun, J.H.; Park, Y.H.; Cho, K.M.; Choi, I.D.; Park, I.M. Manufacturing of Cu-TiB2 composites by turbulent in situ mixing process. *Mater. Sci. Eng. A* **2007**, *449–451*, 1018–1021. [CrossRef]
12. Chen, D.; Jiang, Y.; Li, Y.; Liu, D.; He, J.; Cao, F.; Liang, S. In situ TiB_2/Cu composites fabricated by spray deposition using solid−liquid and liquid−liquid reactions. *Trans. Nonferrous Met. Soc. China* **2020**, *30*, 1849–1856. [CrossRef]
13. Xin, G.A.; Zhou, M.; Jing, K.; Hu, H.; Li, Z.A.; Zhang, Y.; Bai, Q.; Tian, C.; Tian, B.; Li, X.; et al. Heat treatment effects on microstructure and properties of Cu–Ti–Fe alloys. *Mater. Sci. Eng. A* **2024**, *892*, 146068. [CrossRef]
14. Mondi, R.K.; Golla, B.R. Processing and characterization of super strong and wear resistant Al–5Cu-(0-20 vol%)ZrB_2 composites. *J. Alloys Compd.* **2020**, *814*, 152323. [CrossRef]
15. Zhao, J.; Wu, X.; Ning, L.; Zhang, J.; Han, C.; Li, Y. Wetting of aluminium and carbon interface during preparation of Al-Ti-C grain refiner under ultrasonic field. *Ultrason. Sonochem.* **2021**, *76*, 105633. [CrossRef]
16. Arunkumar, T.; Selvakumaran, T.; Subbiah, R.; Ramachandran, K.; Manickam, S. Development of high-performance aluminium 6061/SiC nanocomposites by ultrasonic aided rheo-squeeze casting method. *Ultrason. Sonochem.* **2021**, *76*, 105631. [CrossRef]
17. Tonry, C.E.H.; Djambazov, G.; Dybalska, A.; Griffiths, W.D.; Beckwith, C.; Bojarevics, V.; Pericleous, K.A. Acoustic resonance for contactless ultrasonic cavitation in alloy melts. *Ultrason. Sonochem.* **2020**, *63*, 104959. [CrossRef]
18. Yang, H.; Bu, Y.; Wu, J.; Fang, Y.; Liu, J.; Huang, L.; Wang, H. High strength, high conductivity and good softening resistance Cu-Fe-Ti alloy. *J. Alloys Compd.* **2022**, *925*, 166595. [CrossRef]
19. Wang, Y.; Song, Y.; Fan, Y.; Zhao, H.; Hong, Z.; Song, K.; Dong, X.; Guo, C. Double-peak precipitation hardening in the Cu-Fe-Ti alloy. *Scr. Mater.* **2023**, *232*, 115478. [CrossRef]
20. Zhang, J.; Zhang, S.; Cao, X.; Li, L.; Yang, X.; Chen, Z.; Guo, E.; Kang, H.; Li, R.; Wang, T. Effect of temperature on mechanical behavior of Cu–Cr–Co–Ti alloys. *Mater. Charact.* **2023**, *200*, 112904. [CrossRef]
21. Li, L.; Kang, H.; Zhang, S.; Li, R.; Yang, X.; Chen, Z.; Guo, E.; Wang, T. Microstructure and properties of Cu-Cr-Zr (Mg) alloys subjected to cryorolling and aging treatment. *J. Alloys Compd.* **2023**, *938*, 168656. [CrossRef]
22. Shi, G.; Chen, X.; Jiang, H.; Wang, Z.; Tang, H.; Fan, Y. Strengthening mechanisms of Fe nanoparticles for single crystal Cu–Fe alloy. *Mater. Sci. Eng. A* **2015**, *636*, 43–47. [CrossRef]
23. Yang, H.; Li, K.; Bu, Y.; Wu, J.; Fang, Y.; Meng, L.; Liu, J.; Wang, H. Nanoprecipitates induced dislocation pinning and multiplication strategy for designing high strength, plasticity and conductivity Cu alloys. *Scr. Mater.* **2021**, *195*, 113741. [CrossRef]
24. Li, R.; Kang, H.; Chen, Z.; Fan, G.; Zou, C.; Wang, W.; Zhang, S.; Lu, Y.; Jie, J.; Cao, Z.; et al. A promising structure for fabricating high strength and high electrical conductivity copper alloys. *Sci. Rep.* **2016**, *6*, 20799. [CrossRef]
25. Yu, X.; Song, Y.; Wang, C.; Gu, K.; Zheng, L.; Qiu, W.; Liu, B.; Gong, S.; Li, Z. Effect of Mg content on the microstructure and properties of high strength, high conductivity Cu–Fe–Cr–Si–Mg alloy. *Mater. Sci. Eng. A* **2023**, *883*, 145510. [CrossRef]
26. Choi, E.-A.; Lee, S.J.; Ahn, J.H.; Choe, S.; Lee, K.H.; Lim, S.H.; Choi, Y.S.; Han, S.Z. Enhancement of strength and electrical conductivity for hypo-eutectic Cu-12Ag alloy. *J. Alloys Compd.* **2023**, *931*, 167506. [CrossRef]
27. Manoylov, A.; Lebon, B.; Djambazov, G.; Pericleous, K. Coupling of Acoustic Cavitation with Dem-Based Particle Solvers for Modeling De-agglomeration of Particle Clusters in Liquid Metals. *Metall. Mater. Trans. A* **2017**, *48*, 5616–5627. [CrossRef]
28. Li, J.; Lu, S.; Wu, S.; Gao, Q. Effects of ultrasonic vibration on microstructure and mechanical properties of nano-sized SiC particles reinforced Al-5Cu composites. *Ultrason. Sonochem.* **2018**, *42*, 814–822. [CrossRef]
29. Yang, X.; Wu, S.; Lu, S.; Hao, L.; Fang, X. Refinement of LPSO structure in Mg-Ni-Y alloys by ultrasonic treatment. *Ultrason. Sonochem.* **2018**, *40*, 472–479. [CrossRef]
30. Li, J.; Li, F.; Wu, S.; Lü, S.; Guo, W.; Yang, X. Variation of microstructure and mechanical properties of hybrid particulates reinforced Al-alloy matrix composites with ultrasonic treatment. *J. Alloys Compd.* **2019**, *789*, 630–638. [CrossRef]
31. Xie, Z.; Jiang, R.; Li, X.; Zhang, L.; Li, A.; He, Z. Microstructural evolution and mechanical properties of TiB_2/2195 composites fabricated by ultrasonic-assisted in-situ casting. *Ultrason. Sonochem.* **2022**, *90*, 106203. [CrossRef] [PubMed]
32. Huang, C.; Jiang, Y.; Wu, Z.; Wang, M.; Li, Z.; Xiao, Z.; Jia, Y.; Guo, H.; Niu, L. Significantly enhanced high-temperature mechanical properties of Cu-Cr-Zn-Zr-Si alloy with stable second phases and grain boundaries. *Mater. Des.* **2023**, *233*, 112292. [CrossRef]
33. Zhang, S.; Kang, H.; Wang, Z.; Guo, E.; Chen, Z.; Wang, T. Microstructure and properties of dual-scale particulate reinforced copper matrix composites with superior comprehensive properties. *J. Alloys Compd.* **2020**, *860*, 157888. [CrossRef]

34. Alizadeh, M.; Beni, H.A. Strength prediction of the ARBed Al/Al_2O_3/B_4C nano-composites using Orowan model. *Mater. Res. Bull.* **2014**, *59*, 290–294. [CrossRef]
35. Cheng, M.; Zhang, S.; Liu, Z.; Cao, F.; Jiang, Y.; Chen, Z.; Kang, H.; Guo, E.; Liang, S.; Wang, T. In-situ synthesis of TiB_2 particulate reinforced copper matrix composites with ultrasonic vibration treatment. *Mater. Lett.* **2023**, *335*, 133823. [CrossRef]

Disclaimer/Publisher's Note: The statements, opinions and data contained in all publications are solely those of the individual author(s) and contributor(s) and not of MDPI and/or the editor(s). MDPI and/or the editor(s) disclaim responsibility for any injury to people or property resulting from any ideas, methods, instructions or products referred to in the content.